Experimental study of characteristics of bimetallic Pt-Fe nano-particle fuel cell electrocatalyst

Jun Yao[1] and Yufeng Yao[2*]

[1]University of Lincoln, Brayford Pool, Lincoln LN6 7TS, UK

[2]University of the West of England, Coldharbour Lane, Bristol BS16 1QY, UK

***Corresponding author, yufeng.yao@uwe.ac.uk, Tel: 0044 (0)117 32 87084**

Abstract

The characteristics of 1.5 wt% Platinum (Pt) loading on Fe incorporated Y zeolite (Pt-Fe/Y zeolite) nano-electrocatalysts have been experimentally studied by the extended X-ray adsorption fine structure (EXAFS) and cyclic voltammetry (CV) techniques using Nafion® bound electrode to determine Pt electrocatalytic performance in direct methanol fuel cell. The Pt particle size was found to be small in electrochemical environment (0.7 nm with 55 atoms). Study implies that the Pt electrocatalytic performance can be affected by the Pt cluster electron deficiency, due to the change of Pt particle size associated with the lattice strain energy. The CV measurement in the hydride region indicated higher Pt dispersion for Pt-Fe/Y zeolite electrocatalyst chemically reduced in H_2 at 400°C (15PtFeancr4), compared to that of Pt/Y zeolite reduced at 400°C (15Ptancr4) and Pt-Fe/Y zeolite electrocatalysts reduced at 300°C (15PtFeancr3), respectively. This provided further implication that the chemical reduction temperature would be important for achieving a higher Pt dispersion. The present study has revealed two possible electron transfer pathways that might contribute to the Pt electronic conduction: (1) the surface mobility of adsorbed species; (2) the hydrogen atoms/H^+ ion spillover through the zeolite framework and on the electrode surface, despite the DC insulator nature of zeolite.

Keywords: Bimetallic nano-particle fuel cell, Pt-Fe/Y zeolite, Electrocatalytic performance, Bonding distance, Extended X-ray adsorption fine structure, Cyclic voltammetry (CV).

1. Introduction

Fuel cell has been widely used as an alternative clean energy converting device for many applications, such as mobile phone, portable laptop and hybrid car, because of its unique properties such as zero/low emission, high energy efficiency, and potentially high power density [1, 2]. However, the high cost and short lifespan of Pt as electrocatalyst materials represent two major technical challenges that slow down the progress of fuel cell commercialization, especially for domestic applications. So far, the most promising fuel cell electrocatalyst is the high-loading carbon supported Pt [3, 4]. In recently studies, zeolite has been used as Pt supported substrate in cathode proton exchange membrane (PEM) fuel cell [5, 6] and also as electrode for methanol oxidation, in which the Pt particle size has played an important role in improving the fuel cell electrochemical oxidation and reduction activity [7]. While it was reported that the Pt catalytic activity could be enhanced with increase in Pt surface area [8], there was little understanding on the contribution of protons or auxiliary metal ions (e.g. Fe) as chemical anchors to improve Pt dispersion thus to reduce the Pt particle size and to enhance the electron/charger transfer between Pt and Pt on the metal supporting substrate (i.e. zeolite framework) under electrochemical control. These issues will be addressed in this study.

Based on zeolite structure characteristics, metal particles can be stabilised on zeolite Br∅nsted active sites through the interaction with protons or auxiliary metal ions, such as Fe^{2+}/Fe^{3+} in the interconnected microchannels, and also cages of microporous material, such as NaY zeolite [9]. In a Pt-Fe bimetallic system, strong interactions between Fe ions and zeolite substrates can further stabilize the Pt particles at zeolite surface by anchoring Pt on zeolite active sites to prevent the sintering of Pt metal particles at high temperature in order to achieve a highly dispersed Pt state [10]. Moreover, the catalytic performance of a Pt-Fe zeolite catalyst system can be largely enhanced compared to that of a Pt zeolite catalyst. It was revealed by Hwang and Chung [11] that the specific activity in a Pt-Fe bimetallic system might be partially altered due to the change of Pt-Fe local density resulting in the narrowing of the metal d-band in molecular orbit, rather than being directly influenced by the Pt-Fe particle size. The locations of Pt and Fe particles are also crucially dependent on the stoichiometry of the titration method (O_2, H_2) [11].

It was known that in a gas atmosphere, the metal alloy behaviour could be greatly affected by O_2 and H_2 due to the presence of high reactivity being driven towards the zeolite surface. The Hydrogen chemisorption presents

a major chemical process to control Pt particle size during the Pt calcination and reduction process [12]. As a result, Pt particles can remain in the zeolite supercages at a temperature of 300^{o}C with measured particle sizes between 6Å and 13Å. However, Rolison et al. [13] has observed larger Pt particle sizes of greater than 2nm. Their study indicated that the Pt could migrate into sodality cages and hexagonal prisms at H_2 reduction temperatures of 600+^{o}C, and remain in a stable status inside the sodality cages, particularly in the hexagonal prisms with high charge density. A previous study of using the extended X-ray adsorption fine structure (EXAFS) [10] has predicted the contraction of Pt–Pt bonding distance on zeolite with the following observations: (1) increase in Pt-Pt bonding energy with electron deficiency, leading to a change in local density between the zeolite substrate and the Pt-Fe particle; (2) decrease in the overlapping of metal d-band among the Pt and Fe elements. A further study [14] also revealed that additional Pt atom thermal disorder and Pt-Pt bonding energy increase might lead to an increase in Pt particle size, and consequently a reduction in Pt electro-catalytic performance.

The study of Fe^{2+}/Fe^{3+} ion oxidation/reduction on zeolite indicates that Fe^{2+} ion favourably remained in zeolite supercages [15, 16]. An enrichment of Fe^{2+} at the zeolite surface was mainly attributed by the particle size related high lattice strain energy (see, e.g. [10]). In contrary, the Fe^{3+} ion with high charge density would more likely migrate to small channels, leading to the blockage of zeolite sodalite cages and hexagonal prisms. The Pt entrapped in zeolite cages can form particle size ranging from a single atom [13] to a cluster of 10 to 25 atoms of average 1 - 2 nm in size [17].

Despite these findings, the electronically conducting mechanism of Pt or Pt bimetallic particle on zeolite in an electrochemical environment is still not well understood. The most common hypothesis of electrocatalytic reaction in Pt zeolite system is the H^+ ion 'spillover' pathway, which might involve electrocatalytic reaction on a Nafion$^{@}$ based Pt zeolite electrode due to the nature of zeolite ionic conduction. Furthermore, the hydrogen ‘spillover’ in a Pt zeolite electrode system may interact with not only the Br∅nsted site but also the Lewis site of the zeolite, in which protons act as a catalytic active site for catalysed acidic reaction [18]. The surface diffusion and the ‘spillover’ of H-ad atoms associated with oxygen-containing surface species provide another pathway to promote the electrochemical reaction in addition to the pathway of surface conductance. The electrocatalytic process on Pt zeolite carbon mixed porous electrodes implicated by the cyclic voltammetry (CV) measurement has supported the assumption made on the charge associated Pt zeolite surface

conductance, which involves the acidic oxide species on the carbon surface [19]. Meanwhile, the electrochemical potential regime has significant impact on the surface conductivity pathway and the hydrogen/oxygen 'spillover' pathway in an electrode system, in which the electrode surface condition may be changed. In a Pt/Co electrode system, hydrogen (H^+) ions and oxygen-containing surface species can cause the 'spillover' at the Pt surface. Nevertheless, the Pt-Fe/Y zeolite catalyst may adopt a similar electrocatalytic pathway of H^+ ion 'spillover'. It was found that a 'spillover' phenomenon occurred when the electrochemical reaction took place during the surface diffusion process of absorbed species [18], leading to the migration of hydrogen ions (H^+). Furthermore, the surface conductivity may possibly involve in the electrochemical process since the zeolite is an ionic conductor. In this regard, the hydrogen 'spillover' pathway in a Pt-Fe/Y zeolite electrode system has not been fully understood and thus more researches are required in the field.

In this study, the Fe^{2+} ion is chosen as an auxiliary metal to study the Pt migration in a Nafion$^{@}$ bound zeolite electrode system for highly dispersed Pt distributions. The effect of auxiliary metal functions of Fe^{2+}/Fe^{3+} on Pt particle size and Pt-Fe, Pt-Pt neighbouring distances in a Pt-Fe Zeolite system will be investigated using EXAFS technique in a hydrogen/oxygen gas purged cell and in a electrochemical cell with H_2SO_4 electrolyte solution. The CV measurement will also be performed to ascertain the Pt electrocatalytic activity associated with the hydrogen adsorption/desorption peaks in the hydride region. Finally, experimental results will be analysed to reveal the Pt zeolite electrochemical conducting mechanism in Pt/Y or Pt-Fe/Y zeolite carbon powder Nafion$^{@}$ bound electrode system, and to authors' knowledge this has not been fully explored in published literatures.

2. Experimental

2.1 Preparation of Pt-Fe Y zeolite Electrocatalysts

The 1.5 wt% Pt loading Pt/Y zeolite and Pt-Fe/Y zeolite electrocatalysts were prepared in the Laboratory environment, where the Fe^{2+} underwent ion exchange with zeolite ion in the acidic solution stirred by an ultrasonic bath. The sample was then fully dried and calcined at 350 ^{o}C in a fluidised bed purged with gas air. The resultant sample subsequently underwent ion exchange with the $Pt(NH_3)_4(NO_3)$ solution at neutral pH until no Pt ions in the ion exchanged solution is detected by UV spectroscopy [20]. The final Pt-Fe zeolite products were dried overnight in an oven after being washed by triple distilled water.

The synthesis of Pt or Pt-Fe alloy microstructures on Y zeolite followed the calcination and reduction procedure developed by Gallezot and his co-workers [21]. This involves the removal of Pt and Fe coordinated ligand, i.e. Pt/Y and Pt-Fe/Y zeolite electrocatalysts were purged with argon at a moderate temperature in a fluidized bed reactor fitted with 10 μm pore glass frit. For 1.5 wt% Pt loading Pt-Fe zeolite sample, the calcination process was carried out in O_2 at 350 ^oC, followed by H_2 reduction at 300^oC (denoted as 15PtFeancr3) and 400 ^oC (denoted as 15PtFeancr4), respectively. The 1.5 wt% Pt loading on Y zeolite electrocatalyst was calcined at 350 ^oC in O_2 and later reduced at 400 ^oC in H_2 (denoted as 15Ptancr4).

2.2 Electrochemical cell and cyclic voltammetry

The electrode was made of Pt-Fe/Y zeolite and (untreated) XC-72R carbon powder mixtures added with 15 wt% Nafion$^@$ (i.e. 5 wt% solution in Aliphatic Alcohols and H_2O from Aldrich) conductive electrolytic polymer as a binder. The resultant 'hot' paste was pressed on carbon paper (E-TEK TGHP-90) for solidification. A disc of 2.5cm diameter of electrode was then cut for cyclic voltammetry measurement using a glass-jacketed electrochemical cell, consisting of working Pt electrode and Hg/Hg_2SO_4 Mercury/Mercurous Sulfate (MMS) reference electrodes incorporated with a Pt gauze counter electrode. A 1.3 cm diameter working electrode was later adopted for the EXAFS measurement.

The in-situ EXAFS measurement was carried out in an electrochemical cell formed by two acrylic discs with two Kapton windows cut in the middle, in which a working electrode was placed by one acrylic disc accomplished by a gold wire current collector placing underneath the Pt-Fe/Y zeolite working electrode to reinforce the contact in the cell system via Pt gauze. The Pt-Fe/Y zeolite working electrode was kept within several layers of filter papers soaked in 1 mol dm^{-3} H_2SO_4 solution to prevent the electrode drying out. The Hg/Hg_2SO_4 MMS reference electrode was then connected to the electrochemical cell via a salt bridge, re-assembled to produce a sufficiently large absorption edge for EXAFS measurement.

The electrolyte was 2.5 mol dm^{-3} sulphuric acid (H_2SO_4) solution used for Laboratory cyclic voltammetry measurement and 1 mol dm^{-3} sulphuric acid (H_2SO_4) for the in-situ EXAFS measurement using a computer-controlled potentiostat (Auto-Lab PGSTAT20), respectively. The working electrode was controlled by a

potential ramp from waveform generator at a constant scan rate (dE/dt) of 1 mV/s [22]. The oxidation/reduction of the electro-active species of interest on Pt-Fe/Y zeolite electrode was detected by a current change in the potential region of -0.65 V to 0.5 V, in which no solvent and electrolyte decomposition occurred [23].

2.3 Extended X-ray adsorption fine structure (EXAFS)

The Extended X-ray Absorption Fine Structure (EXAFS) measurements were performed using the Synchrotron Radiation Source (SRS) at Daresbury Laboratory, UK. The wiggler beam line was operated at 2 GeV and 100 mA, and the high-order harmonics that may affect the amplitude of EXAFS were removed using a double-crystal Si220 monochromator. The 50% detuning of a harmonic beam was used to locate the Pt L_{III} absorption edge, e.g. using gas - ion chambers filled with Ar, Xe or Kr and He. A Pt foil was used as a reference sample for EXAFS data collection.

Data analysis was carried out using software EXCALIB, EXBROOK and EXCURV 98. The inter-atomic distance, atom number and type of backscattering neighbours were determined, based on following equations as [24]

$$A_j(k) = (N_j / 2k\ R_j) S_0^2 F_j(k) e^{-2k^2\sigma_j^2} e^{-2R_j/\lambda(k)}, \quad (1)$$

$$\chi_k = \sum_{j=1}^{shell} (N_j / 2k\ R_j) S_0^2 F_j(k) e^{-2k^2\sigma_j^2} e^{-2R_j/\lambda(k)} \sin[2kR_j + 2\phi_{absorbance}(k) + \phi_{backscattered}(k)], \quad (2)$$

$$FT(r) = 1/\sqrt{2\pi} \int_{\min}^{k_{\max}} k^n \chi(k) \exp^{(-2ikr)}\, dk, \quad (3)$$

where N_j is the number of neighbouring atoms of type j with backscattering amplitude $F_j(k)$, which is dependent on the neighbouring atom number. S_o is an amplitude reduction term that takes into account the body effect such as shake-up and shake-off process due to multi-electron excitation and energy loss [24]. The term $e^{-2k^2\sigma_j^2}$ is the Debby Waller factor which represents a measurement of static and thermal disorder in the sample and is temperature dependent. $\lambda_j(k)$ is the mean free path length of the photo electron. ϕ is the

outgoing and backscattering electron wave function of the core atomic potentials of the emitting atom and backscattered atom. X_k is the function of EXAFS. k is measured in $Å^{-1}$. A_j is the wave amplitude.

3. Results and Discussion

3.1 Zeolite BET surface areas measurement

The Brunauer-Emmett-Teller (BET) surface area measurement and X-ray diffraction (XRD) characterization were employed primarily to investigate the change of zeolite crystalline structure. Figure 1 depicts the zeolite BET surface area measurement for the three electrocatalysts 15Ptancr4, 15PtFeancr3 and 15PtFeancr4, respectively. The measurement of a plain zeolite sample was used for reference, in which the surface area of 632 m^2g^{-1} was determined. For Fe incorporated catalysts with 1.5wt% Pt loading on zeolite either reduced at 300 ^oC (i.e. 15PtFeancr3) or at 400 ^oC (i.e. 15PtFeancr4), the surface areas of two zeolite samples were very close and measured at 371 m^2g^{-1} and 346 m^2g^{-1}, respectively. This is almost twice as large as the value (168 m^2g^{-1}) given by the catalyst with 1.5 wt% Pt loading on zeolite reduced at 400 ^oC (i.e. 15Ptancr4). While compared to the plain zeolite surface area, the discrepancy is about 261 - 286 m^2g^{-1}. The BET measurement indicates that the surface area of zeolite crystallized structure of the Fe incorporated Pt zeolite electrocatalysts (both 15PtFeancr3 and 15PtFeancr4) is preserved relatively well, in comparison to that of Pt zeolite electrocatalyst (i.e. 15Ptancr4). The reduction of zeolite surface area indicates that the collapse of crystallized zeolite structure is predominant during the calcination and reduction process, leading to the blockage of zeolite opening pores in small channels. This has been further confirmed by X–ray diffraction (XRD) measurements, as presented in figure 2.

The XRD data were collected by using an impinging or a reflected X-ray beam at an incident angle of 2-Theta (θ) in a range of 5^o – 44^o at room temperature. The XRD measurements were primarily used to qualitatively examine the zeolite crystalline structure changes due to thermal treatment with metal disposition. Comparing to that of a standard plain zeolite [25], the XRD pattern has shown a significant reduction of the diffraction peak intensity by a maximum factor of 10 for sample 15Ptancr4 and a maximum factor of 100 for Fe incorporated samples 15PtFeancr3 and 15PtFeancr4, together with a slight ‘shift’ of peak positions. The XRD

pattern baseline and noise level of spectra for Fe incorporated Pt zeolite catalysts is found to be very high, which indicates a structure disorder resulting from the 'collapse' of the zeolite crystallite structure. The XRD spectra exhibit similar patterns for all types of Pt and Pt-Fe/Y zeolite electrocatalysts studied. As the Pt deposition quantity is relatively small, the decrease of zeolite surface area may imply the blockage of the smaller pores owing to the collapse of zeolite structures during the calcination and reduction process, particularly for Fe incorporated Pt catalysts (i.e. 15PtFeancr3 and 15PtFeancr4). Conclusively, the XRD spectra have confirmed the BET surface area measurements for zeolite structural change [25]. Table 1 displays a comparison of zeolite surface area of the corresponding electrocatalysts. It can be seen that the zeolite surface area for 1.5wt% Pt/Y zeolite electrocatalyst (i.e. 15Ptancr4) is the smallest, implying that the 'collapse' of zeolite crystalline structures might be severe, compared to Fe incorporated samples 15PtFeancr3 and 15PtFeancr4.

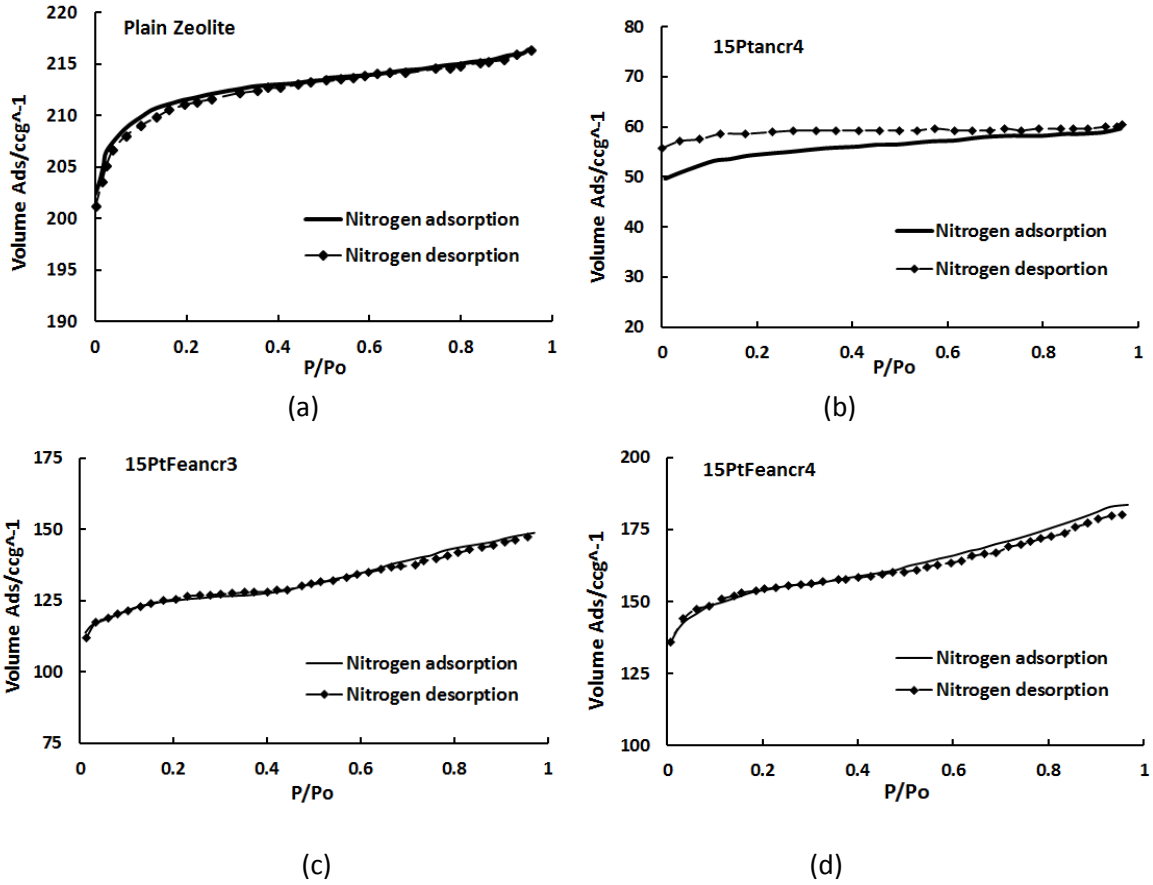

Figure 1. Volumetric uptake of Nitrogen at 77K with absorption in solid lines, and desorption in solid line with symbols. (a) plain zeolite; (b) 1.5 wt% Pt loading on zeolite calcined at 350 ^{o}C and reduced at 400 ^{o}C (15Ptancr4); (c) 1.5 wt% Pt loading on Fe incorporated zeolite calcined at 350 ^{o}C and reduced at 300 ^{o}C (15PtFeancr3); (d) 1.5 wt% Pt loading on Fe incorporated zeolite calcined at 350 ^{o}C and reduced at 400 ^{o}C (15PtFeancr4).

Table 1. The BET surface area measurements for plain zeolite, Pt zeolite and Fe incorporated Pt zeolite electrocatalysts. The measurement error is between 0.1% and 10%.

Acronym Name	Surface Area m^2/g
Plain Zeolite Catalyst	$623.2 \pm 0.1\%$
15Ptancr4 Catalyst	$168 \pm 10\%$
15PtFeancr3 Catalyst	$371 \pm 5.0\%$
15PtFeancr4 Catalyst	$346 \pm 3.0\%$

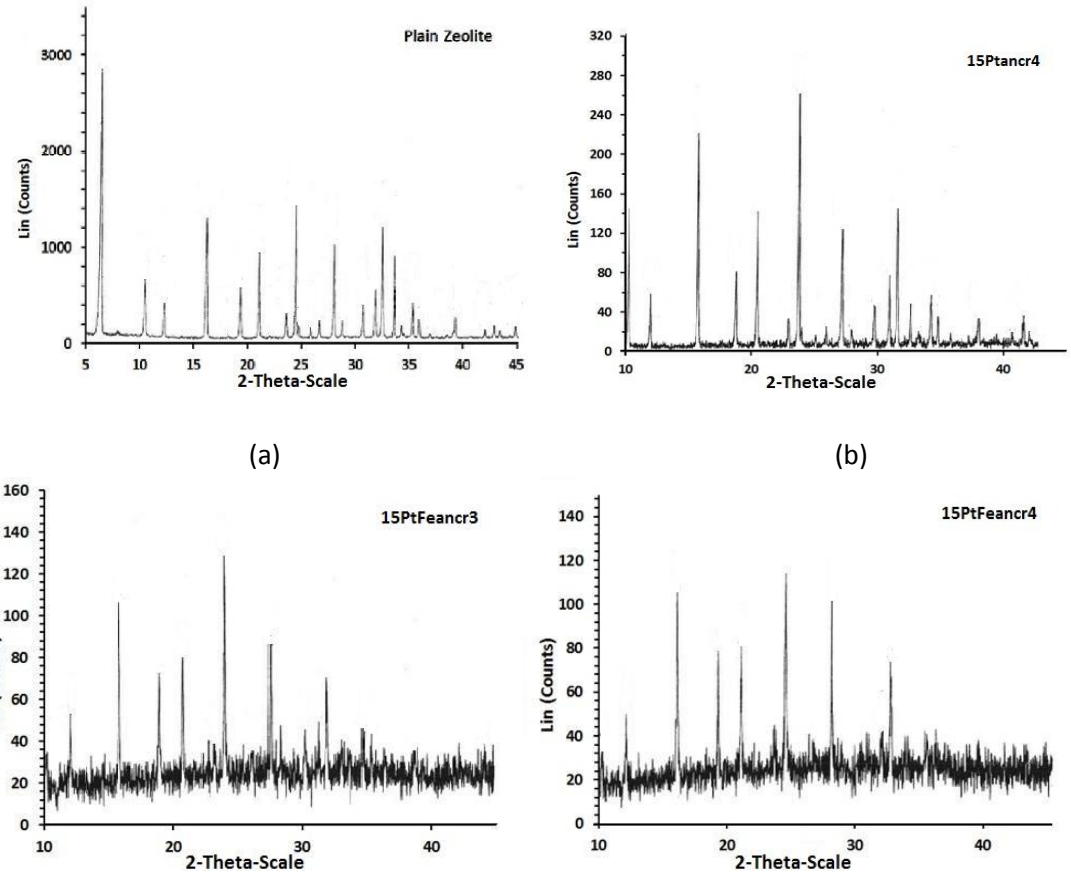

Figure 2. The X-Ray Diffraction (XRD) patterns, (1) plain zeolite; (2) 15Ptancr4; (3) 15PtFeancr3; (4) 15PtFeancr4. Theta (θ) is the Bragg angle of incidence or reflection of the X-ray beam, and Lin (counts) is the unit of X-ray intensity.

3.2 The ex-situ EXAFS measurement for 1.5 wt% Pt electrocatalyst on zeolite (15Ptancr4) without Fe

3.2.1 1.5 wt% Pt loading Pt/Y zeolite electrocatalyst

The pellet was employed for the ex-situ EXAFS measurement using 1.5 wt% Pt Y zeolite and boron nitride powder mixture. It was placed between two pieces of plastic film in O_2 or H_2 purged gas cell at room temperature. The EXAFS spectrum was taken at the Pt L_{III} edge and was then analysed using a computer code EXCURV 98 developed at Daresbury Laboratory, UK.

Figure 3 depicts the k^3 weighted EXAFS (Chi) data and its Fourier transforms (FT) presented in R-space. The dotted symbols represent fitted results of the raw data. The amplitude of Chi data of sample 15ancr4 collected in O_2 tends to exhibit insignificant oscillation. A maximum peak in R-space was found to be 2.76Å in the Fourier transform (FT) spectrum, and a higher neighbouring shell was fitted at a peak value between 4Å and 6Å. Also the Pt-O bonding distance in R-space is determined to be 2.02Å in the first Pt-O shell and the correspondent oxygen number is approximately 1.23. The Pt-Pt distance in the second Pt shell is predicted to be about 2.76Å. This closely resembles the metal Pt-Pt bonding distance, indicating a crystallographic network of Pt particles, similar to that of Pt metal foil, which was used as background reference sample during data collection.

A progressive increase in the high *k*-value of the raw EXAFS spectrum amplitude and oscillation has been determined by samples with 1.5 wt% Pt loading on Y zeolite (i.e. 15Ptancr4) in hydrogen purged gas cell (see Fig. 3b). This suggests that Pt nano-particle has a longer neighbouring distance and a high *z*-value (i.e. atom number) in neighbouring field within a short oscillation period. There is no neighbouring oxygen atom predicted and the Pt–Pt distance at the Pt first shell was measured to be 2.75Å, indicating the metallic nature of Pt nano-particles with the face centered cubic (FCC) structure of Pt metal. The Pt-Pt coordination number (N) in the first shell was 6.33, a factor of 2 higher than a number of 3.13 predicted for the same sample treated in gas cell purged with O_2 (i.e. shell 2 in Table 2a). In both cases, the Pt has fitted up to 4 shells. The overall Pt-Pt coordination numbers fitted for data collected in H_2 cell (as seen in Table 2b) has 17 atoms, compared with average number of 14.83 atoms fitted for data collected in O_2 cell. The results are in good agreement with that given by Benfield [26]. In another similar study [27], the Pt-Pt coordination number was found to be 6.0 for a Pt/Y sample calcined at 300 ^{o}C and reduced at 500 ^{o}C. This value also agrees well with that from the present study for 1.5 wt% Pt on Y zeolite (i.e. 15Ptancr4).

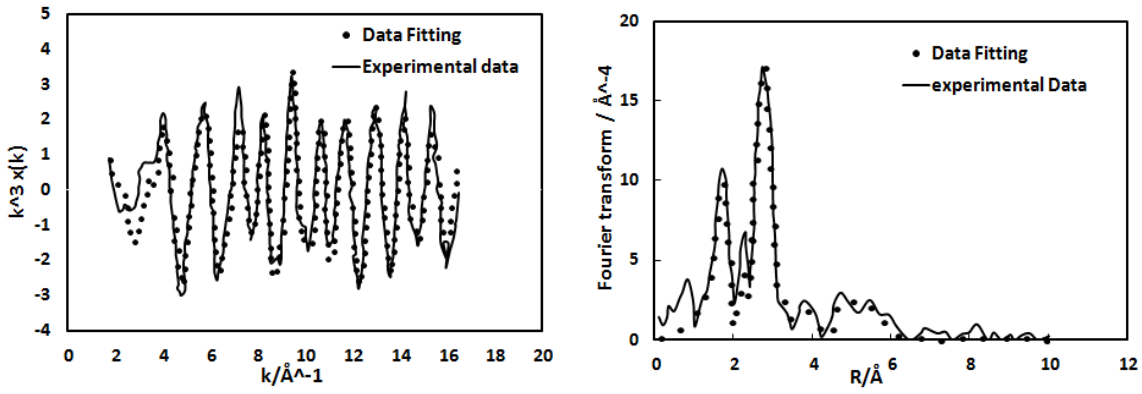

(a) In Oxygen gas

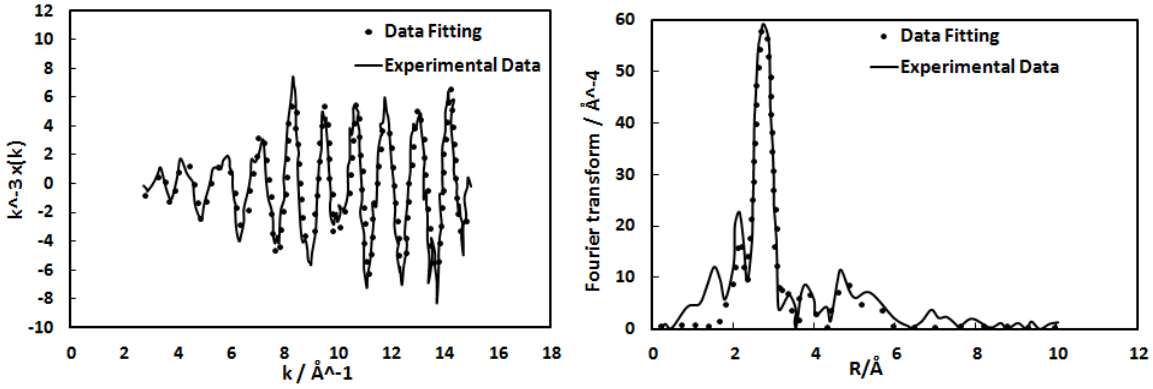

(b) In Hydrogen gas

Figure 3. EXAFS data fitting for 1.5 wt% Pt loading Pt/Y zeolite catalysts (a) Data collected in gas cell purged by Oxygen, with phase correction; (b) Data collected in gas cell purged by Hydrogen, with phase correction. The experimental data are in solid lines and the fitted data are in dotted symbols, respectively. The EXAFS data was collected at Pt L_{III} edge. Sample 15Ptancr4 - calcined at 350 ^{o}C and reduced at 400 ^{o}C (i.e. 15Ptancr4).

Table 2. Data fitting results for each Pt shell at Pt L_{III} edge

(a) Data fitting results for sample 15Ptancr4 in O_2 gas at room temperature

15ancr4	Shell 1 - O	Shell 2 - Pt	Shell 3 - Pt	Shell 4 - Pt	Shell 5 - Pt
N	1.23	3.13	1.75	3.12	6.83
R (Å)	2.02	2.76	3.90	4.81	5.44

(b) Data fitting results for sample 15Ptancr4 in H_2 gas at room temperature

15ancr4	Shell 1 - Pt	Shell 2 - Pt	Shell 3 - Pt	Shell 4 - Pt
N	6.33	0.88	3.34	6.40

R (Å)	2.75	3.91	4.78	5.42

3.2.2 1.5 wt% Pt loading with Fe incorporated Pt-Fe zeolite electrocatalyst

3.2.2.1 Analysis of ex-situ EXAFS data collected at Pt L_{III} edge in O_2 at room temperature

The effect of auxiliary Fe^{2+} ions in assisting the Pt distribution on zeolite framework has been investigated using the EXAFS spectroscopy at Pt L_{III} edge and at Fe K-edge, in oxygen or hydrogen purged gas cell, respectively.

Figure 4 illustrates the EXAFS spectra and Fourier transforms, fitted in R-space by k^3 weighting for 1.5 wt% Pt loading catalyst on Fe incorporated Y zeolite purged in either O_2 or H_2. The data fitting results are shown in table 3.

A high noise level was found in the Chi data spectrum for 1.5 wt% Pt loading Pt-Fe metal alloy zeolite electrocatalyst calcined at 350 ^{o}C and reduced at 300 ^{o}C (i.e. 15PtFeancr3) and 400 ^{o}C (i.e. 15PtFeancr4), respectively, compared with that of 1.5 wt% Pt loading of Pt/Y zeolite electrocatalysts (i.e. 15Ptancr4). A high oxidation state was detected in sample 15PtFeancr3 with a correspondent O_2 coordination number of 0.92. The neighbouring coordination number of Pt and Fe are 1.26 and 0.54, respectively. The averaged Pt-O bonding distance is predicted about 1.99Å for sample 15Ptfeancr3 and 1.94Å for sample 15PtFeancr4, respectively, both having slightly shortened distances compared to a normal Pt-O bonding distance of 2.02Å in O_2 gas. It was found that the Pt fitting in the second shell had not shown similar agreement with those found in sample 15Ptancr4. A contraction of Pt-Pt bonding distance is predicted at 2.56Å and 2.57Å for sample 15PtFeancr3 and for sample 15PtFeancr4, respectively, compared to 2.76Å for 1.5 wt% Pt loading on Y zeolite (i.e. 15Ptancr4). As observed and discussed by Mathew [28], the shortening of Pt bonding distance is possibly attributed to an additional third shell of Fe in the metal to form a Pt-Fe bimetallic particle, and this could result in a 'shift' of d-band energy to reduce the distance of the Pt-Pt bond in Fourier transform module. The Pt-Fe bonding distance is found 2.44Å for sample 15PtFeance4 and 2.59Å for sample 15PtFeancr3, respectively. The additional second shell fitting of Pt for sample 15PtFeancr4 has led to an improvement of a fitting value R_{exafs} to 47.73% with the Pt-Pt distance predicted at 3.99Å, and the Pt coordination number is measured to be 1.55 in shell 1 and 1.00 in shell 2 correspondent to Fe and O_2 coordination numbers of 0.65 in shell 3 and 0.75 in

shell 1. The high neighbouring oxygen atom coordination number predicted for sample 15PtFeancr3 indicates the incomplete reduction of Pt or Fe oxides at a moderate reduction temperature of 300 ^{o}C resulting in lower quality of EXAFS data, as implied by a fitting value R_{exafs} of 59.71%.

For sample 15PtFeancr4, the multiple Pt shells of data fitting indicates that high percentage of Pt or Pt-Fe alloy is located on the zeolite exterior surface at a relatively high reduction temperatures. The Pt particle reduced at 400 ^{o}C (i.e 15PtFeancr4) in H_2 gas may be more likely to remain in zeolite supercages or on zeolite external surfaces in comparison to that reduced at a relatively low temperature of 300 ^{o}C (i.e. 15PtFeancr3). Other researchers also obtained similar findings, i.e. a small fraction of metal particles was distributed on the exterior of zeolite with little constrain from the internal architecture of zeolite structure [14, 29]. For Pt located at the interior of the zeolite framework, an electron deficiency of Pt cluster has been observed previously [13] due to the formation of a metal-proton adduct on zeolite acidic sites. The auxiliary metal ions, such as Fe^{2+} ion has similar functionality as the proton in a zeolite system, where they assist in anchoring the Pt particle onto the zeolite cage wall during the precursor thermal treatment. The Fe^{3+} ions are more favourable to remain in the zeolite small cages, such as sodalite cages and hexagonal prism than the Fe^{2+} ion due to their high charge density. The formation of a mixed oxidation phase by Fe^{2+} and Pt^{2+} ions can prevent the mobility of Pt-Fe bimetallic alloy and thus leads to an increase in Pt distribution of zeolite. A further improvement of Pt stability is also possible, and can be initiated by the interference of Pt and acidic oxidising species on zeolite surface [10].

On the other hand, Pt^{2+} ions in smaller cages are possibly migrating back to the zeolite supercages at relatively high reduction temperatures. The adducting ability of Fe ion may contribute to the contraction of Pt–Pt bonding distance by higher Pt and Fe binding energy resulting in the enhancement of Pt particle dispersion on zeolite external/interior surface. It was found that in general the Pt particle size on zeolite (i.e. 15PtFeancr3 and 15PtFeancr4) is relatively small in the presence of Fe^{2+}/Fe^{3+}, compared with 1.5 wt% Pt loading on zeolite without Fe ion incorporated sample (i.e 15Ptancr4).

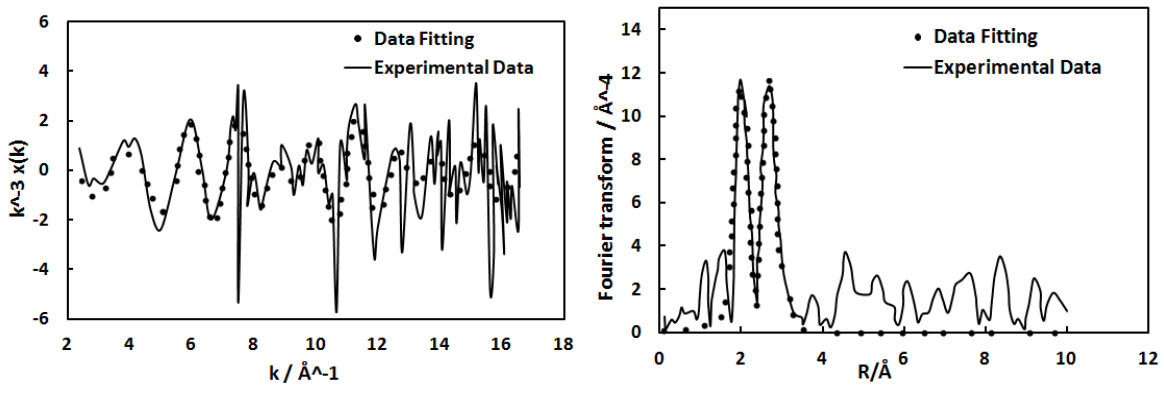

(a) Sample 15PtFeancr3 in O_2

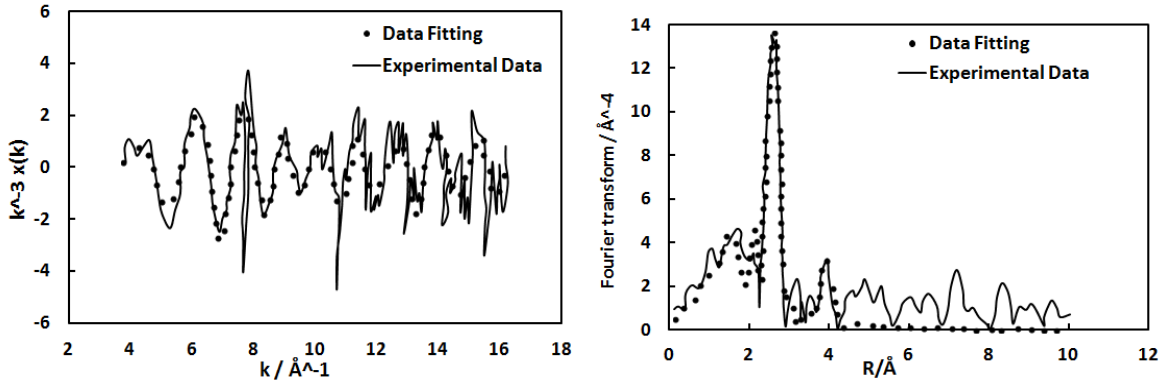

(b) Sample 15PtFeancr4 in O_2

Figure 4: Comparison of EXAFS experimental raw data (in solid lines) and the fitted data (in dotted symbols) for 1.5 wt% Pt loading Pt-Fe Y zeolite catalysts in O_2 purged gas cell with phase correction. The EXAFS data was collected at Pt L_{III} edge. (a) Sample 15PtFeancr3 - calcined at 350 ^{o}C and reduced at 300 ^{o}C (i.e. 15PtFeancr3); (b) Sample 15PtFeancr4 - calcined at 350 ^{o}C and reduced at 400 ^{o}C (i.e. 15PtFeancr4).

Table 3. The EXAFS data fitting results, collected at Pt L_{III} edge in O_2 purged gas cell at room temperature for sample 15PtFeancr3 and sample 15PtFeancr4, respectively.

15PtFeancr3	Shell 1 - O	Shell 2 - Pt	Shell 3 - Fe
N	0.92	1.26	0.54
R (Å)	1.99	2.57	2.59

15PtFeancr4	Shell 1 - O	Shell 2 - Pt	Shell 3 - Fe	Shell 4 -Pt
N	0.75	1.55	0.65	1.00
R (Å)	1.94	2.56	2.44	3.99

3.2.2.2 Analysis of ex-situ EXAFS data at the Pt L_{III} edge in hydrogen gas at room temperature

The Pt structure was analysed using EXAFS data collected at Pt L_{III} edge in hydrogen at room temperature. The improvement of EXAFS (Chi) data noise level is clearly visible with no Pt-O bond predicted, indicating a significant reduction of Pt samples in hydrogen. The breaking up of Pt-O bond could be due to the replacement of oxygen by Fe to form a new Pt-Fe bimetallic bond. The second shell of Pt was predicted with a coordination number of 3.82 for Fe incorporated sample with 1.5wt% Pt loading on zeolite, which was calcined at 350 ^{o}C and reduced at 300 ^{o}C (i.e 15PtFeancr3) or 400 ^{o}C (i.e 15PtFeancr4), as illustrated in Figure 5. The corresponding Pt-Pt bonding distance was determined at 2.71Å and 2.70Å, respectively (see Table 4). The Pt-Pt bonding distances are slightly shortened while compared with the Pt metallic bonding distance of 2.75Å and also those observed in 1.5 wt% Pt loading Y zeolite system with no Fe presence (i.e. 15Ptancr4). The Fe local coordination number in the first shell was estimated to be 1.35 for sample 15PtFeancr3 and 1.51 for sample 15PtFeancr4 with associated Pt-Fe bonding distances of 2.62Å and 2.59Å, respectively. It can be seen that the Fe particle size increases with the increase in reduction temperature. Also no oxygen atom was predicted, which indicates that the Fe-Pt bimetallic particles were fully reduced in Hydrogen, and that the shortening of Pt-Pt bonding distance may be due to the increase of Pt binding energy and the Pt atom electron deficiency as a result of by metal particle polarization.

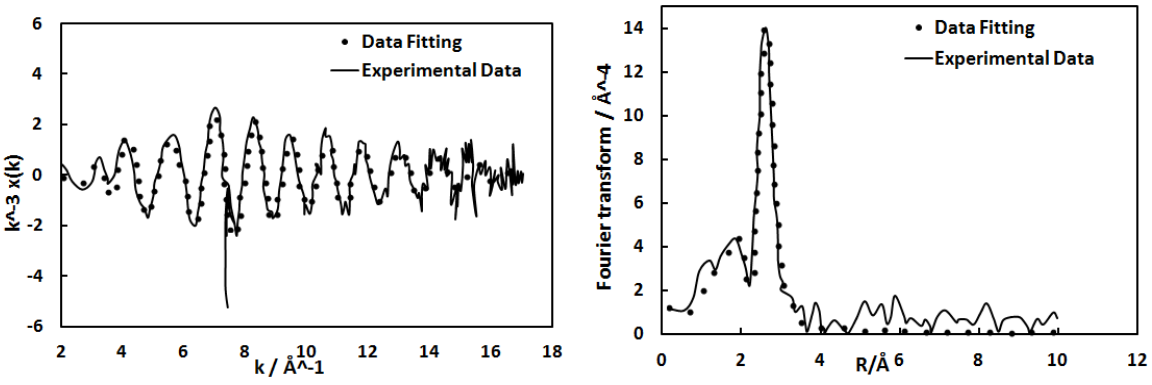

(a) Sample 15PtFeancr3 in hydrogen

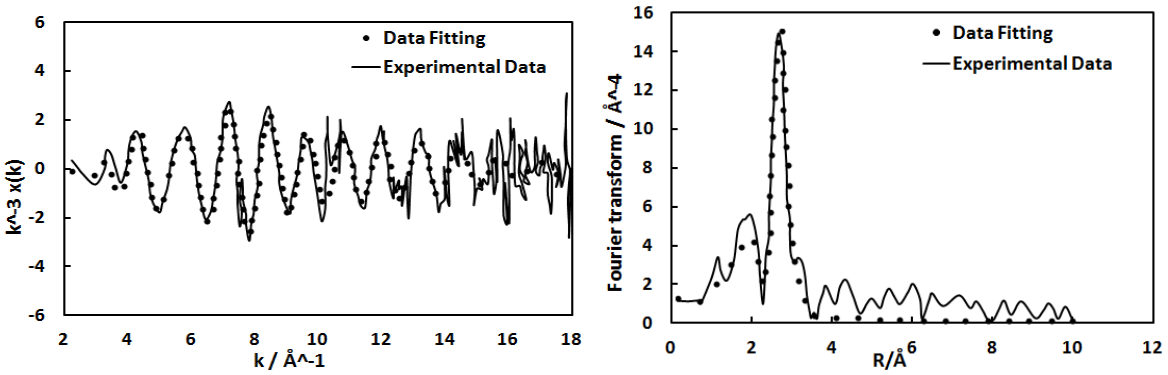

(b) Sample 15PtFeancr4 in hydrogen

Figure 5. EXAFS data fitting for 1.5 wt% Pt loading Pt on Fe incorporated Y Zeolite catalysts in hydrogen with phase correction. The experimental data are presented in solid lines and the fitted data shown in dotted symbols, respectively. The EXAFS data was collected at Pt L_{III} edge. (a) Sample 15PtFeancr3 - calcined at 350 ^{o}C and reduced at 300 ^{o}C; (b) Sample 15PtFeancr4 - calcined at 350 ^{o}C and reduced at 400 ^{o}C.

Table 4. EXAFS data fitting results for data collected at Pt L_{III} edge in hydrogen gas at room temperature corresponding to sample 15PtFeancr3 and sample 15PtFeancre4, respectively.

15PtFeancr3	Shell 1 - Fe	Shell 2 - Pt
N	1.35	3.82
R (Å)	2.62	2.71

15PtFeancr4	Shell 1 - Fe	Shell 2 – Pt
N	1.51	3.82
R (Å)	2.59	2.70

3.2.2.3 The ex-situ EXAFS data analysis for sample collected at Fe K-edge in O_2 gas at room temperature

The analysis continues for EXAFS data collected at Fe K-edge in order to restate evidences found at Pt L_{III} edge and to determine the metallic Fe-Pt oxides. The oxygen atom coordination number in shell 1 is predicted as 2.04 for sample 15PtFeancr3 and 1.4 for sample 15PtFeancr4, and the associated Fe-O distance is 1.95Å and 1.91Å, respectively. An extra 'O' coordination number was found in shell 4 with coordination number of 4.35

for 15PtFeancr3 and 3.24 for 15PtFeancr4, respectively indicating strong oxidation of Pt-Fe metal alloy. A significant increase in the Fe-Fe coordination number is predicted at 0.92 (compared to 0.54 at Pt L_{III} edge) for sample 15PtFeancr3 and 1.27 (compared to 0.65 at Pt L_{III} edge) for sample 15PtFeancr4 with the increased inter-atomic distance of 2.45Å (vs 2.59Å at Pt L_{III} edge) and 2.38Å (vs 2.44Å at Pt L_{III} edge). The Pt coordination number was predicted to be 0.95 (vs 1.26 at Pt L_{III} edge) and 1.90 (vs 2.55 at Pt L_{III} edge) for Fe associated Pt samples in comparison. The discrepancy of coordination number and inter-atomic distance between fitted EXAFS data collected at Pt L_{III} edge and at Fe K-edge may be attributed by the noise level in EXAFS raw data. The significant shortening of Fe bonding distance compared to that of a standard Fe-Fe bonding distance of 2.65Å is probably caused by differences in the atom charge density between Pt and Fe. However, no major contraction of Pt bonding distance was found.

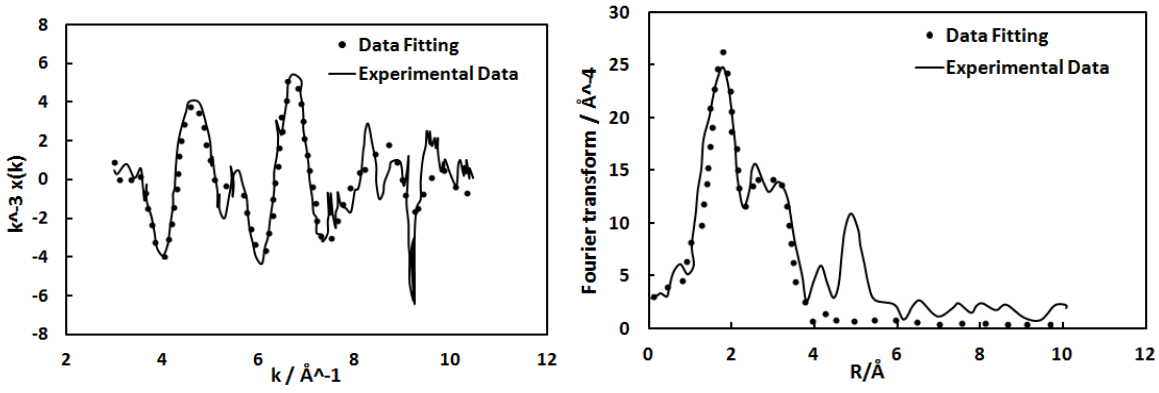

(a) Sample 15PtFeancr3 in O_2

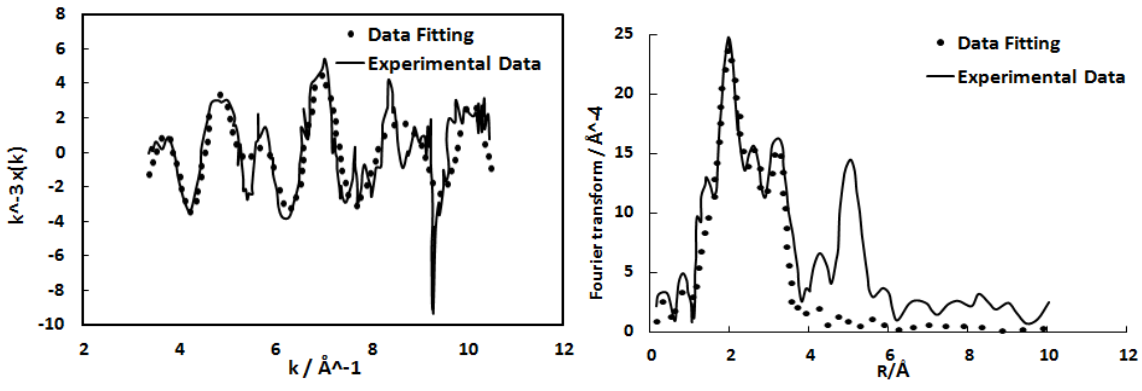

(b) Sample 15PtFeancr4 in O_2

Figure 6. EXAFS data fitting for 1.5 wt% Pt-Fe/Y zeolite electrocatalyst samples in O_2 with phase correction. The experimental data are displayed in solid lines and the fitted data presented in dotted symbols, respectively. The EXAFS data was collected at Fe K-edge. (a) 15PtFeancr3 - 1.5 wt% Pt loading on Fe incorporated Y zeolite

calcined at 350 ^{o}C and reduced at 300 ^{o}C; (b) 15PtFeancr4 - 1.5 wt% Pt loading on Fe incorporated Y zeolite calcined at 350 ^{o}C and reduced at 400 ^{o}C.

Table 5. EXAFS Data fitting results, data collected at Fe K-edge in O_2 gas at room temperature for samples 15PtFeancr3 and 15PtFeancre4, respectively.

15PtFeancr3	Shell 1 - O	Shell 2 - Fe	Shell 3 – Pt	Shell 4 - O
N	2.04	0.92	0.95	4.35
R (Å)	1.95	2.45	2.72	3.36

15PtFeancr4	Shell 1 - O	Shell 2 - Fe	Shell 3 - Pt	Shell 4 - O
N	1.40	1.27	1.90	4.84
R (Å)	1.91	2.38	2.72	3.24

3.3 The cyclic voltammetry (CV) measurement

The cyclic voltammetry (CV) measurement was performed in an electrochemical cell to determine the electro-activity of species in the electrolyte solution using Nafion$^{@}$ bound electrode made by the mixture of Fe incorporated Pt electrocatalyst on Y zeolite and carbon powder. The response of an electrochemical reaction was determined by monitoring current change with potential. The CV measurement of a 1.5 wt% Pt loading on Pt/Y zeolite carbon | Nafion$^{@}$ electrode (i.e. 15Ptancr4) and a 1.5 wt% Pt/C | Nafion$^{@}$ electrode (i.e. 15Pt/XC-72R) made from a commercially available 40wt% Pt/XC-72R carbon catalyst mixed with the extra XC-72R carbon, is depicted in Figures 7a-7b, to investigate the hydrogen adsorption/desorption activity on Pt surface at -0.65 V in 2.5 mol dm^{-3} H_2SO_4 solution.

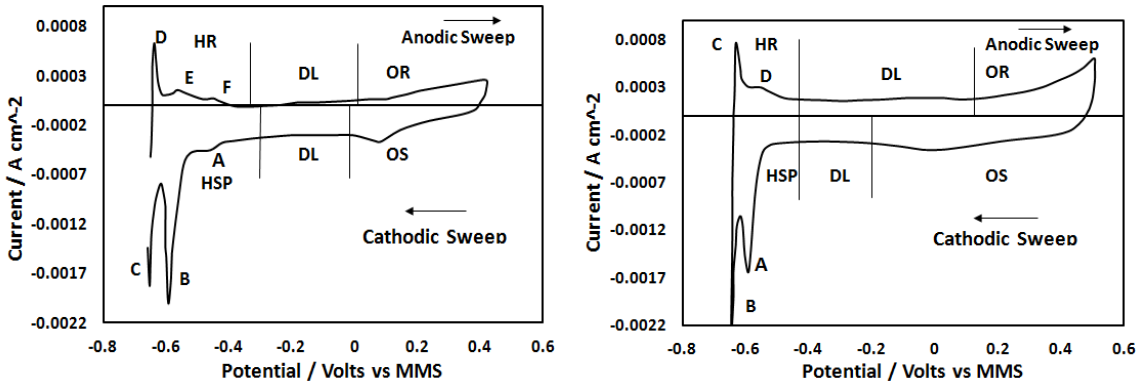

(a) (b)

Figure 7. The steady state CV curves are measured at a scan rate of 1 mV/s in 2.5 mol dm^{-3} H_2SO_4 solution. (a) 1.5 wt% Pt/XC-72R electrode prepared by a mixture of 40 wt% Pt/XC-72R with extra plain XC-72R carbon powder (i.e. 15Pt/XC-72R), (b) 1.5 wt% Pt/Y zeolite (i.e. 15Ptancr4) made with extra plain XC-72R carbon powder.

The CV lines consist of three distinguished regions, namely hydride region comprising hydrogen adsorption (HSP)and hydrogen reduction (HR) regions; oxide reduction (OR) and oxide Stripping (OS) regions; and the double layer region (DL), respectively. For the 1.5 wt% Pt/XC-72R electrode (i.e. 15Pt/XC-72R) (as seen in Figure 7a), the hydrogen adsorption potential (HSP) of the hydride region starts at -0.32 V and goes down to -0.65 V, where a strong adsorption of H^+ ions occurs at the peak 'B'. This is attributed by the high H_2 adsorption energy on the plane of the Pt and also electron conduction between Pt and Pt, with the peak 'C' being responsible for a hydrogen evolution at -0.65V. The peak 'A' is linked with the weakly adsorbed H^+ ions forming covalent bonds on Pt catalytic sites. The H re-oxidation of the peak 'D' is observed in the anodic sweep of potential from -0.65 V to -0.36 V, and the peaks 'E' and 'F' represents weakly and strongly bound H desorption sites, respectively. A current increase at the potential oxidation region (OR) of 0.12 V to 0.5 V indicates the formation of Pt oxide species at Pt electrode surface, while an oxide stripping (OS) occurs at the cathodic sweep in a potential region of 0.5 V to -0.02 V. A charger separation between the Pt metal surface and the electrolyte solution was predicted to occur in a double layer (DL) region from 0.02 V to -0.36 V and -0.36 V to 0.12 V in a reverse sweep manner.

Figure 7b displays a typical CV of 1.5 wt% Pt/Y Zeolite carbon mixed Nafion@ bound working electrode (i.e. 15Ptancr4), with the electrochemical oxidation and reduction features similar to that on 1.5 wt% Pt/XC-72R

Nafion@ bound electrode. The potential sweep region was confined between -0.65 V and 0.5 V at a slow sweep rate of 1 mV/s. The Pt nano-particles electrochemical activity was predicted to occur in the hydride region between -0.45 V and -0.65 V in both cathodic and anodic sweep directions. Hydrogen adsorption peak, representing a strong Pt bounded catalytic site (peak 'A'), has been observed at -0.6 V, and no weakly bounded Pt catalytic site was determined. It is possible that both weakly and strongly bounded hydrogen may adsorb similar amount of energy, resulting in difficulties to distinguish them unless a much slower sweep rate, e.g. less than 1 mV/s, being used. Further decrease in potential to -0.65 V leads to hydrogen evolution, as illustrated by (peak 'B'). The re-oxidation of hydrogen (peak 'C') was determined at -0.64 V, and sole hydrogen desorption peak 'D' was detected at -0.56 V. An oxidation current in the anodic sweep was recorded in a potential range from 0.15 V to 0.5 V, and oxygen was stripped in a potential region of 0.5 V to -0.2 V in the direction of cathodic sweep. A small peak predicted at 0 V is probably due to the removal of Pt oxides.

The electron transfer of hydrogen adsorption/desorption in the hydride region on Pt active site follows the reaction equations below:

Cathodic reaction	$H^+ + e^- \rightarrow H_{adsorption}$		(4)
Anodic reaction	$H_{adsorption} \rightarrow H^+ + e^-$		(5)
Hydrogen evolution	$2H_{adsorption} \rightarrow H_{2(g)}$		(6)
Overall reaction	$2H^+ + 2e^- \rightarrow H_{2(g)}$		(7)

The Pt surface oxidation/reduction due to H_2O is represented below:

$Pt + H_2O \rightarrow OHPt + H^+ + e^-$		(8)
$OHPt \rightarrow PtO + H^+ + e^-$		(9)
$PtO + H^+ \rightarrow Pt + OH^-$		(10)
$PtO + 2H^+ \rightarrow Pt + H_2O$		(11)

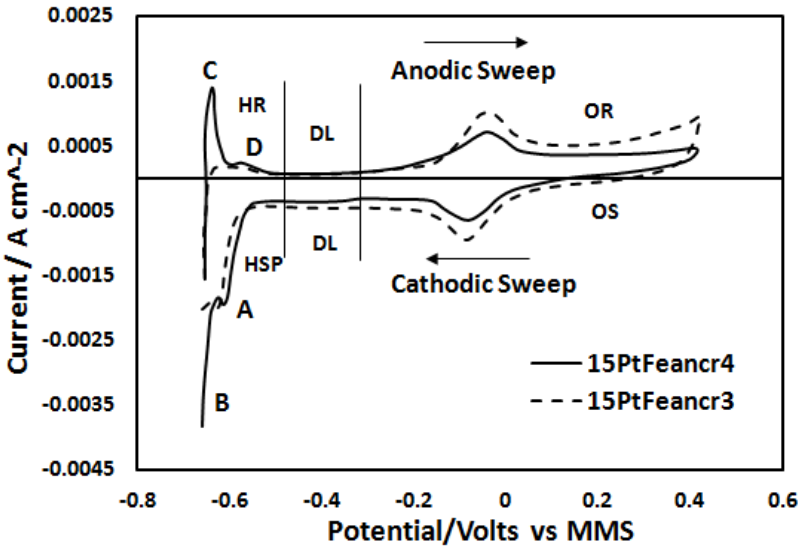

440

441 Fig. 8. Steady state CVs are measured in a 2.5 mol dm^{-3} H_2SO_4 solution at a scan rate of 1 mV/s. The dashed line
442 represents the CV measurement for sample 15PtFeancr3, and the solid line is the CV measurement for sample
443 15PtFeancr4.

444

445 Figure 8 depicts the electrocatalytic activity of 1.5 wt% Pt-Fe/Y Zeolite | Nafion@ working electrode (i.e.
446 15PtFeancr3 and 15PtFeancr4) at the potential region between +0.5 V and -0.65 V. The CV curve consists of
447 very different electrochemical behaviour with only two distinguished regions associated with hydrogen
448 adsorption/desorption peaks.

449 The current measurement of the double layer (DL) however is consistent in a potential region of -0.5 V to -0.35
450 V. The values of two quasi-reversible peaks are determined at 0.2 V and 0.1 V, respectively, which indicates
451 the electrochemical oxidation and reduction of Fe^{2+}/Fe^{3+} ion redox surface groups. The high oxidation current
452 change (in dotted line) was measured by the electrode made by 15PtFeancr3 Y zeolite and the current
453 increases in the positive potential region (OR) upon to 0.5 V. This is in good agreement with the EXAFS data
454 regarding a high oxygen coordinate value around Pt for 15PtFeancr3. The oxide stripping (OS) occurs at 0.5 V
455 to -0.2V during the cathodic sweep of the potential. The large current drop (HSP) and the increase (HR) due to
456 hydrogen adsorption (peak 'A') and hydrogen evaluation (peak 'B')/hydrogen re-oxidation (peak 'C') and
457 desorption (peak 'D') in hydride region was predicted for the cell with an electrode made by 15PtFeancr4 (in
458 solid line). This implies that Pt active sites are higher on electrocatalyst 15FePtancr4 than that of 15PtFeancr3.
459 The hydrogen re-oxidation and desorption current is significantly suppressed on an electrode made by

15PtFeancer3, and there is no clear hydrogen re-oxidation and desorption peaks detected. This may be due to similar energy levels of these two sites. The Fe incorporated 1.5 wt% Pt electrocatalyst shows consistent tendency for electrochemical activity, compared with 1.5 wt% Pt/Y zeolite sample (i.e. 15Ptancr4) or 1.5 wt% Pt/XC-72R electrocatalyst made by 40 wt% Pt/XC-72R and extra carbon powder mixture, respectively.

The hydrogen adsorption/desorption peak in hydride region demonstrated the presence of electron/ion transfer at the interface of Nafion@ bound Pt or Pt-Fe zeolite electrode and electrolyte solution. However, Pt electrocatalytic performance depends on Pt particle size and their distribution on zeolite at different thermal treatment conditions. The high Pt active sites were dedicated for sample treated at high reduction temperature (i.e. 15PtFeancr4), compared with sample 15PtFeancr3 treated at relatively low reduction temperature. Based on previous studies of Gallezot et al. [16, 21], the location of Pt^{2+}, Fe^{2+} and Fe^{3+} ions on zeolite depends on the calcination/reduction temperature and metal zeolite surface interaction. The Pt ions are likely to occupy small cages, such as sodalite cages and hexagonal prisms at the calcination temperature of 350+ ^{o}C. The high negative charge density of small cavities may provide a main driving force to move the multivalent metal ions from supercages to sodalite cages, in particular to the hexagonal prisms [30]. On the other hand, Pt particles can more easily migrate backward to the supercages at reduction temperature of 400 ^{o}C instead of temperature of 300 ^{o}C. The small cages can be blocked in the presence of Fe^{3+} during calcination owing to high positive charge density, while the Fe^{2+} ion in the supercages acts to anchor the Pt particles onto the zeolite cage wall [31].

From the study of hydrogen 'spillover' pathway on Pt/C catalyst by Srinivas and Rao [32], it was proposed that the hydrogen adsorption/desorption occurs on carbon based Pt active sites. Later study by McBreen [33] further revealed the current generation on Pt active sites, which are situated remotely from the conducting material surface with fast surface mobility of adsorbed species on the electrode. Therefore, the surface active sites of Pt particles that are not in direct contact with solid conductive polymer electrolytes such as the Nafion@ membrane can involve in an interfacial process through the pathway of surface conductance.

Zeolite material is generally known as an electrical insulator, but it is capable of acting as a solution like ionic conduction [34] and as an electron bank to donate or receive electrons in the presence of the zeolite Br∅nstead or Lewis acidic sites to produce a flow of protons along zeolite acidic sites. This results in two

possible pathways in contribution to the electronic conducting in 1.5 wt% Pt or Pt-Fe bimetallic alloy/Y Zeolite carbon powder | Nafion@ electrode system, either the surface mobility of adsorbed species or hydrogen adatoms/H^+ ion 'spillover' through zeolite framework or on electrode surface [19]. The study of Wen et al. [19] indicates that a hydrogen atom 'spillover' process on Pt/C electrode can occur during the surface diffusion process, in which hydrogen ions (H^+) were able to form OH group with carbon acidic surface oxides where the carbon black was a main substrate of the electrode surface. The study by Fujimoto [35] has revealed H^+ 'spillover' in gas phase on Br∅nsted and Lewis acidic sites where there is a catalytic reaction to take place. Similar process might be adopted to explain the electrochemical conductivity in Pt/Y zeolite or Pt-Fe bimetallic alloy/Y zeolite electrode system, despite that zeolite is an electrical insulator. The Br∅nsted sites on zeolite and phenolic group on carbon materials contain acidic sites/groups, which can be ionized to provide protons and to contribute to the surface conductance.

A 'spillover' pathway may occur during the surface diffusion process of the absorbed species [18]. The H^+ 'spillover' can be transmitted between active sites and along the zeolite substrate surface to increase the surface conductivity of the electrode. In this case, water has played an important role to facilitate hydrogen migration into the Pt catalytic sites on the zeolite framework. Hence, the H^+/hydrogen 'spillover' provides a direct pathway for Pt particle that are not in direct contact with Nafion@ to participate in the electrochemical reaction at the catalyst |Nafion @ interface, and in further strengthening the surface conductivity. The cyclic voltammetry measurement has confirmed that a reversible hydrogen adsorption/desorption peak can be detected in 1.5 wt% Pt-Fe bimetallic alloy/Y zeolite catalysts |Nafion@ electrode system, in agreement with that in well studied Pt/C electrode system. For surface oxygen containing species in 1.5 wt% Pt-Fe/Y zeolite carbon mixed electrode | Nafion@ system, the interfacial electrochemical reaction mainly involves ionic conduction and surface conductivity. Therefore, the effect of ohmic drop is significant. Moreover, the electron transfer may take place between the electrode and solution via free species, such as H^+ and H_3O^+. Ions are transported through the free species by hitching a ride on water during their migration through the small zeolite channels.

3.4 In-situ EXAFS study for 1.5 wt% Pt/Y zeolite and 1.5 wt% Pt-Fe/Y zeolite electrocatalysts

3.4.1 Pt particle structure study for 1.5 wt% Pt/Y zeolite electrocatlyst

Figure 9 illustrates the EXAFS data fitting with the raw Chi data spectra ($k^3\chi(k)$ vs k/Å) and Fourier transform for 1.5 wt% Pt/Y zeolite (i.e. 15Ptancr4) electrocatalyst with correspondent to the fitting results illustrated in Table 6. The in-situ EXAFS data was collected at Pt L_{III} edge at room temperature under the potential deposition of -0.65 V in 1.0 mol dm^{-3} H_2SO_4 solution. The curve fitting (in dotted lines) matches the general form of the raw data (in dashed lines) very well and the data fitting was extended up to 3 shells with shell 1 and shell 2 predicted for Pt and shell 3 for oxygen, respectively. The Pt coordination numbers in shell 1 and shell 2 are approximately 7.45 and 2.05. The introduction of third Pt-O shell data has significantly improved the data fitting quality. A metallic nature of Pt nano-particle is determined with Pt-Pt distance of 2.77Å, which implies the preservation of the bulk of Pt characteristics. The in-situ prediction of Pt-Pt distance in 1.0 mol dm^{-3} H_2SO_4 electrolyte solution is similar to that fitted using ex-situ EXAFS data collected in hydrogen gas cell. As the Pt particle size is small, compared with fitting results for data collected in air and hydrogen gas cells, the Pt-O bond may attribute to either the re-oxidation of Pt at -0.65 V in hydride region or the direct link of Pt associated with oxygen on the Lewis acidic site.

Table 6. The data fitting results for 1.5wt% Pt/Y zeolite (i.e. 15Ptancr4) electrocatalyst under potential deposition of -0.65 V in hydride region in 1.0 mol dm^{-3} H_2SO_4 solution.

15Ptancr4	Shell 1 - Pt	Shell 2 - Pt	Shell 3 - O
N	7.45	2.05	0.75
R/ Å	2.77	3.85	2.19

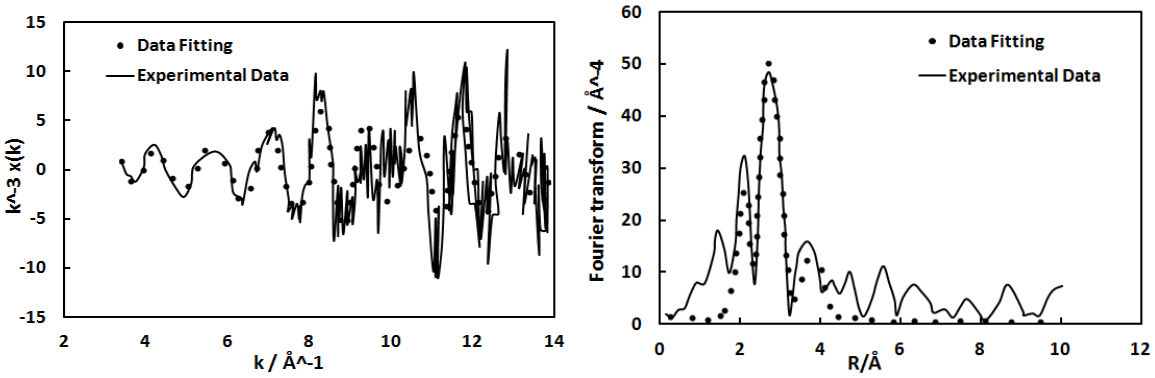

(a) Chi data (b) Fourier transformation

Figure 9. EXAFS data fitting for 1.5 wt% Pt Y zeolite catalysts with phase correction (i.e. 15Ptancr4). The experimental data and the fitting results are presented in solid lines and dotted symbols, respectively. Data is collected at a potential of -0.65 V vs MMS reference electrode in 1.0 mol dm^{-3} H_2SO_4 solution under potential deposition. The EXAFS data was collected at Pt L_{III} edge.

3.4.2 Pt particle structure study for Fe incorporated 1.5 wt% Pt loading on Y zeolite

The Fe incorporated Pt particle structure on zeolite is characterised by using in-situ EXAFS technique, in which EXAFS data was collected at the Pt L_{III} edge with 1.5 wt% Pt loading on Y zeolite incorporated with Fe ions (i.e. 15PtFeancr3 and 15PtFeancr4) under a potential deposition of -0.65 V in 1.0 mol dm^{-3} H_2SO_4 electrolyte solution. Figure 10 depicts the fitted EXAFS spectra and the corresponding data are presented in Table 7. The sample 15PtFeancr3 has shown poorer data fitting quality than that of sample 15PtFeancr4. The local Pt coordination number of shell 1 for sample 15PtFeancr3 is approximately 4.87, slightly lower than 5.07 predicted for sample PtFeancr4. The Fe coordination number fitted in shell 2 is 1.96 for sample 15PtFeancr4 and 1.37 for sample 15PtFeancr3, respectively. The average atom numbers of Pt particle in the hydride region has shown a significant increase with a decrease of Pt-Pt (2.72Å) and Pt-Fe (2.53Å or 2.51 Å) bonding distance compared to the Pt-Pt and Pt-Fe distances of 2.75Å and 2.59Å determined by previous en-situ EXAFS data analysis. The shortening of Pt and Fe bonding distance is possibly attributed to high electron deficiency of metal during charger transfer under a potential deposition process at -0.65 V. The fitting results in the hydride region indicate a high distribution of Pt particle for 1.5 wt% Pt loading Fe Y zeolite electrocatalyst system reduced at 400 ^{o}C (i.e. 15PtFeancr4), compared with electrocatalyst reduced at 300 ^{o}C (i.e. 15PtFeancr3). The high current change in hydride region observed by cyclic voltammetry measurement (as seen in figure 8) has

demonstrated a high level of coverage of Pt active sites of zeolite for catalyst of 15PtFeancr4. The current change in hydrogen adsorption/desorption region for catalyst 15PtFeancr3 is relatively low, implying a low coverage of Pt active sites.

Table 7. EXAFS data fitting results for Fe incorporated Pt samples. Data were collected at Pt L_{III} edge at -0.65 V under potential deposition in 1.0 mol dm^{-3} H_2SO_4 electrolyte solution.

15PtFeancr3	Shell 1 - Pt	Shell 2 - Fe
N	4.87	1.96
R (Å)	2.72	2.53

15PtFeancr4	Shell 1 - Pt	Shell 2 - Fe
N	5.03	1.37
R (Å)	2.72	2.51

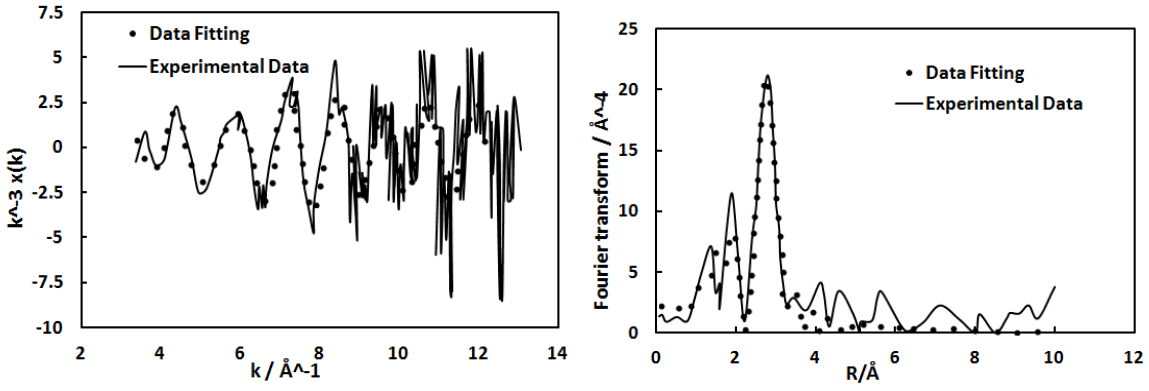

(a) 15PtFeancr3 in 1.0 mol dm^{-3} H_2SO_4 solution

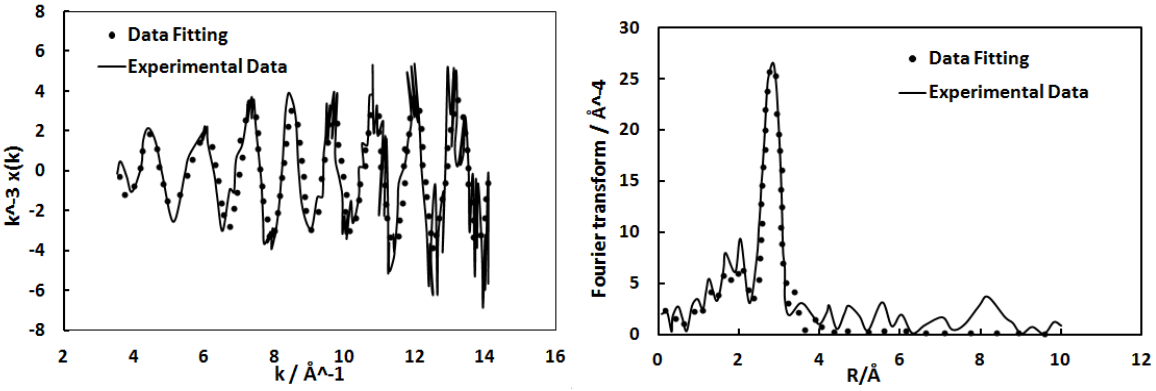

(b) 15PtFeancr4 in 1.0 mol dm^{-3} H_2SO_4 solution

Figure 10. EXAFS data fitting for 1.5 wt% Pt-Fe/Y zeolite catalysts with phase correction. The experimental data and the fitted results are presented in solid lines and dotted symbols, respectively. Data is collected at a potential of -0.65 V vs MMS reference electrode under potential deposition. (a) 15PtFeancr3 - 1.5 wt% Pt loading on Y zeolite incorporated with Fe calcined at 350 ^{o}C and reduced at 300 ^{o}C; (b) 15PtFeancr4 - 1.5 wt% Pt loading on Y zeolite incorporated with Fe calcined at 350 ^{o}C and reduced at 400 ^{o}C.

4. Pt distribution on zeolite

4.1 Estimation of Pt particle size and Pt distribution

Based on the Benfield theory [26], the Pt cluster size and geometry can be estimated using the mean value of the first nearest neighboring coordination number $\overline{N_i}$ of atoms in a cluster, as a function of cluster edge length. The formula for $\overline{N_i}$ is derived from two geometric models, i.e. icosahedron and cubo-octahedron. It is assumed that Pt structure for Pt zeolite catalysts has an icosahedral model, as illustrated in figure 11. This is because an icosahedral cluster might be more metallic than that of cubo-octahedral model with same atom numbers. Subsequently, the total number of atoms N_{total} in a cluster and the average first – nearest neighboring coordination number $\overline{N_i}$ can be calculated numerically using following formulae, based on the number of Pt shells in a cluster:

$$N_{total} = (1/3)(2m-1)(5m^2-5m+3) \quad (12)$$

$$\overline{N_i} = 6[(m-1)(20m^2-25m+12)]/[(2m-1)(5m^2-5m+3)] \quad (13)$$

where *m* represents the complete Pt shell number.

Table 8 illustrates the number of Pt atoms and the average first nearest neighboring coordination number in a Pt cluster for Pt zeolite catalysts in hydrogen reduction.

For Fe incorporated Pt zeolite, a simplified formula can be used to calculate mean coordination number $\overline{N_i}$ of a cluster containing Pt and Fe atoms follows equation 14 below.

$$\overline{N_i} = \overline{N_i}(Pt-Pt) + \overline{N_i}(Pt-Fe) \quad (14)$$

Table 8. Pt atoms mean first nearest neighboring coordination number in a Pt cluster.

Acronym Name	Catalyst 15Ptancr4	Catalyst 15PtFeancr3	Catalyst 15PtFeancr4
$\overline{N_i}$ from refinement - Pt	6.33	5.17	5.33

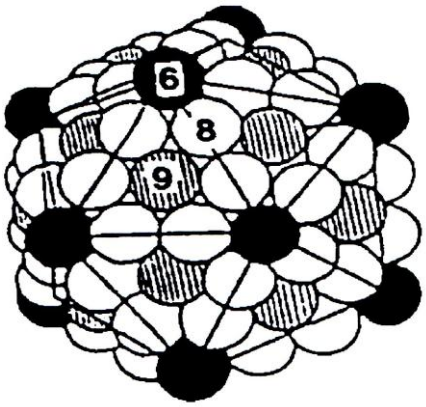

Figure 11: The icosahedrons structure with 147 atoms (m = 4), where atom 6 represents the vertex atom with 6-coordinate, atom 8 shows the edge atom with 8–coordinate, atom 9 represents the atom with 9-coordinate in the triangular face [26].

The Pt particle size is estimated at 0.7 nm for 1.5 wt% Pt loading on zeolite with 55 atoms in Fe incorporated samples (i.e. 15PtFeancr3 and 15PtFeancr4) and at 1 - 1.1 nm for 1.5 wt% Pt loading on zeolite with 147 atoms in a Pt cluster. Previous cyclic voltammetric measurement has shown a high surface area distribution of Pt for Fe incorporated Pt zeolite catalyst, indicating a highly dispersed Pt particle surface area on zeolite due to the presence of Fe^{2+} ions. As Sachtler et al. suggested [12], Fe^{2+} cation in zeolite channel can be oxidized to Fe^{3+} during the calcination process, as Fe^{3+} ions are more likely to migrate into zeolite small cages (i.e. sodalite cages and hexagonal prisms) due to high charge density. The mobility of Pt ions can be restrained by Fe^{2+} ions in supercages and zeolite external surface as a result of anchoring Pt on the zeolite cage wall.

4.2 Pt active surface area and distribution on electrode surface

The actual Pt loading can be calculated by following equations, in which the edge jump is obtained from EXAFS data subtraction.

$$In(I / I_o) = \mu x \quad , \tag{15}$$

$$m = (\mu x) * (S) / (\mu / \rho) \quad , \tag{16}$$

where μ is the total linear absorption coefficient (cm^{-1}) for the primary beam, defined by the natural log of the ratio of the transmitted photon intensity (I) and incident intensity (I_o). χ is the thickness of the material. m is

623 total mass of the element interested and S is cross sectional surface area of the pellet or electrode. ρ is the
624 density of the absorbance. The mass absorption coefficient μ/ρ is known to be 179 for Pt at the L_{III} edge at
625 room temperature, and S is 1.327 cm^2.

626 The surface area of Pt particle in direct contact with H_2SO_4 solution can be determined by applying hydrogen
627 adsorption/desorption peak measurement. Table 9 illustrates the comparison of Pt distribution on zeolite for
628 Pt-Fe bimetallic alloy and Pt zeolite catalysts treated at different reduction temperatures.

629 The Fe incorporated Pt zeolite catalyst reduced at 400 ^oC (i.e. 15PtFeancr4) has a significantly high Pt surface
630 area. This has been demonstrated by analyzing the hydrogen adsorption peak due to current charge transfer in
631 the hydride region at the potential between -0.65 V and 0 V. The Pt active surface area is measured at 84.98
632 m^2/g for the Fe incorporated Pt zeolite catalyst reduced at 400 ^oC (i.e. 15PtFeancr4) with 1.54 wt % Pt loading
633 on zeolite. The Fe incorporated Pt zeolite catalyst reduced at 300 ^oC (i.e. 15PtFeancr3) gives a consistent Pt
634 active surface area, compared with the Pt loading on zeolite catalyst reduced at 400 ^oC (i.e. 15Ptancr4). The Pt
635 active surface area is predicted at 55.9 m^2/g with 1.49 wt% Pt loading on zeolite for Fe incorporated sample
636 15PtFeancr3, and 51.29 m^2/g with 1.52 wt% Pt loading for Pt alone sample 15Ptancr4, respectively. The
637 prepared Pt loading on zeolite for all samples studied is consistent with the proposed value of 1.5 wt% Pt
638 loading on Y zeolite.

639 The net Pt atoms per cm^2 predicted for samples 15PtFeancr4, 15Ptancr4 and 15PtFeancr3 are in an order of
640 $5.28\times10^{17} > 5.21\times10^{17} > 5.11\times10^{17}$ per cm^2, respectively. The slightly low number of Pt net atom per cm^2 for
641 sample 15PtFeancr3 may be associated with relatively low Pt loading on zeolite. In general, Pt surface atoms
642 decrease with the decrease of reduction temperature. However, it seems that the Fe incorporated Pt catalyst
643 has resulted in better Pt surface atom dispersion at high reduction temperature, compared to Pt loading with
644 no Fe incorporated zeolite catalyst treated at same condition. The Pt surface atom dispersion for Fe
645 incorporated Pt zeolite sample reduced at 400 ^oC (i.e. 15PtFeancr4) is predicted to be 24.70%, which is
646 significantly higher than that of 16.30% and 14.66% for Fe incorporated Pt zeolite catalyst reduced at 300 ^oC
647 (i.e. 15PtFeancr3) and Pt zeolite catalyst reduced at 400 ^oC without Fe incorporated (i.e. 15Ptancr4). The
648 associated Pt surface atoms per cm^2 on zeolite were determined to be 13.04×10^{16} (i.e. 15PtFeancr4), 8.33

649 $\times 10^{16}$ (i.e. 15PtFeancr3) and 7.64×10^{16} (i.e. 15Ptancr4), respectively. The data indicates a high Pt surface area
650 distribution of 15PtFeancr4, due to relatively small Pt particle size.

651 The present study has shown that Pt distribution in zeolite system is mainly influenced by Fe ions and chemical
652 reduction temperature. A highly dispersed Pt on zeolite can be achieved at high reduction temperature in H_2
653 and result in the formation of Pt and Fe bimetallic bond. The high Pt active surface area that leads to high
654 electrocatalytic activity has been demonstrated by the cyclic voltammetry measurement in 2.5 mol dm^{-3} H_2SO_4
655 electrolyte solution by Nafion$^{@}$ bound Pt-Fe electrode.

656 Table 9. Pt active surface area m^2 per gram and the value of Pt atom distribution in the per cm^2 electrode area.

Catalyst	15Ptancr4	15PtFeancr3	15PtFeancr4
Pt active surface area m^2/g	51.29	55.9	84.98
Calculated mass quantity in wt %	1.52	1.49	1.54
N_T Pt atoms per cm^2 ($\times 10^{17}$)	5.21	5.11	5.28
N_S Pt surface atoms per cm^2 ($\times 10^{16}$)	7.64	8.33	13.04
Dispersion N_S/N_T (%)	14.66	16.30	24.70

657

658 *N_T: total atoms in a cluster; N_S from Benfield theory (i.e. total number of surface atoms in a cluster for
659 samples 15PtFeancr3 and 15PtFeancr4 are 12.)

660

661 A shell-type distribution of Pt particles can be used to understand Pt and Fe dispersion on zeolite for catalyst
662 15PtFeancr4 reduced at 400 ^{o}C. In this case, Fe^{2+} ion acts in a very similar way as H^{+} ion to promote the Pt
663 particle distribution by anchoring Pt on zeolite surface/supercage wall and further to restrict Pt migrations
664 through zeolite microchannel at H_2 reduction temperature of 400 ^{o}C. While the collapse of zeolite
665 microstructures, about 50% decrease of zeolite surface area for Fe incorporated Pt zeolite catalysts could be
666 possible due to the Fe species blockage of the zeolite opening pores, and this agrees well with other published
667 observations [12]. Subsequently, some of Pt particles can be encapsulated in zeolite cages. The in-situ EXAFS
668 data analysis (see, e.g. figure 10 and table 7) has predicted a relatively high Fe atoms distribution close to Pt
669 first shell for catalyst 15PtFeancr3 pre-treated in H_2 gas cell at reduction temperature of 300 ^{o}C. In this case, Fe

has failed to produce a high Pt distribution based on CV measurement of hydrogen coverage of surface area. Both Pt and Fe are more likely encaged inside the zeolite microchannel.. The reduction temperature of 300 ^{o}C is not high enough to enforce Pt and Fe migration back to either zeolite surface or supercage. This leads to the incompletion of reduction of Pt in H_2, unless further increasing the reduction temperature until 400 ^{o}C i.e. like case of catalyst 15PtFeancr4.

5. Conclusion

In this paper, we studied the characteristics of zeolite supported Pt-Fe bimetallic nano-particle and their electrocatalytic performance using EXAFS data analysis and cyclic voltammetry measurements. The electron transfer pathway at small metal particles was also investigated under electrochemical control.

The resultant analysis has led to the proposal of the electron transfer pathways, illustrating the Pt-Fe bimetallic electrocatalytic activity and their electronic conduction via 1.5 wt% Pt loading Pt-Fe/Y zeolite carbon powder | Nafion$^{@}$ bound electrode system. The formation of a mixed Fe oxide phase can prevent metal surface mobility of Pt and lead to increase in Pt distribution of zeolite. A further increase in Pt stability is possible on the formation of the Pt and zeolite oxide interface. It was suggested that Fe^{2+} could act as a proton to anchor Pt on zeolite cage wall and restrain the mobility of Pt on zeolite in chemical reduction process. The strong interaction between Fe^{2+} and zeolite substrate can stabilize the Pt on zeolite surface and prevent the sintering of Pt metal particles at high temperature, leading to a highly dispersed Pt surface area distribution, which is achieved by controlling chemical reduction temperature in H_2 gas cell during calcination and reduction process. Both in-situ EXAFS and cyclic voltammetry measurements indicate that Pt particle has a relatively higher surface area distribution for Pt-Fe zeolite catalysts reduced at 400 ^{o}C in H_2 gas cell (i.e. 15PtFeancr4) than that of Pt zeolite (i.e. 15Ptancr4) or Pt-Fe zeolite electrocatalysts reduced at 300 ^{o}C (i.e. 15PtFeancr3) with a better electrocatalytic performance in hydride region. In general, Pt surface area is high for Pt-Fe zeolite electrocatalyst, compared to that of Pt zeolite electrocatalyst.

696 The Fe^{3+} ions oxidized from Fe^{2+} were favourably located inside the zeolite small cages to block the zeolite
697 channel. A high Pt particle distribution is predicted for Fe incorporated Pt sample reduced at 400 ^{o}C (sample
698 15PtFeance4). The Pt-Pt bonding distance is 2.75Å - 2.77Å, indicating the metallic characteristics of the bulk Pt.
699
700 The Pt particle size on zeolite with Fe incorporated catalyst is relatively small, compared with catalyst without
701 adding a secondary Fe metal. This is evidenced by cyclic voltammetry measurement for hydrogen
702 adsorption/desorption peak in the hydride region via current charge transfer. It was suggested that the H^+ ions
703 'spillover' pathway could be used to depict the electron transfer and Pt electrocatalytic performance in
704 electrolyte solution. The presence of hydrogen species adsorbed on Pt might contribute to either direct
705 electron transfer or the mobility of H_{ads}/H^+ species. Alternatively, ionic and electronic conduction may also
706 occur via free species, such as H^+ and H_3O^+ through which ion is transported by hitching a ride on water during
707 their migration through zeolite channels to increase the electrode surface conductivity.
708
709 Conclusively, this study has confirmed that Pt nano-particles in Y zeolite system can be electrochemically
710 accessed on Nafion$^{@}$ bound electrode made by Pt zeolite or Pt-Fe zeolite despite the DC insulation of zeolite.
711 The Pt electrocatalytic performance can be improved by adding a secondary metal such as Fe element. The
712 cyclic voltammetry and EXAFS measurements also show chemical oxidation and reduction temperature is
713 crucial to achieve high Pt dispersion on zeolite. Conclusively, Fe incorporated Pt catalyst as a new type of
714 electrocatalyst exhibits some promises for fuel cell applications to reduce the cost as well as to enhance the
715 fuel cell efficiency.
716

717 ## 6. References

718 1. S. Litster, G. Mclean, 'PEM fuel cell electrodes,' Journal of Power Sources, 130(1), (2004), 61 - 76.
719 2. H.N. Yang, J.Y. Lee, Y. Na, S.C. Yi, W.J. Kim, 'Effect of functionalization for carbon molecular sieve (CMS)
720 synthesized using zeolite template on the incorporation of Pt nanoparticle and performance of the electrodes
721 in PEMFC,' Microporous and Mesoporous Materials, 152, (2012), 148 - 156.

722 3. H.A. Gateiger, S.S. Kocha, B. Sompalli, F.T. Wagner, 'Activity benchmarks and requirements for Pt, Pt-alloy,
723 and non-Pt oxygen reduction catalysts for PEMFC,' Appl. Catal. B: Environ. 56, (2005), 9-35.
724 4. C.J. Zhong, J. Luo, P.N. Njoki, D. Mott, B. Wanjala, R. Loukrakpam, S. Lim, L. Wang, B. Fang, Z. Xu, 'Fuel Cell
725 Technology: Nano-Engineered Multimetallic Catalysts,' Energy Environ. Sci., 1, (2008), 454 - 466.
726 5. Y. R.J. Thomas, M. M. Bruno, H. R. Corti, 'Characterization of a monolithic mesoporous carbon as diffusion
727 layer for micro fuel cells application,' Microporous and Mesoporous Materials, 155, (2012), 47-55.
728 6. J.Y. Lee, Y.H. Yun, S.W. Park, S.D. Kim, S.C. Yi, W.J. Kim, 'Synthesis of nano-sized Pt/C via zeolite-templating
729 method and its application to the cathode catalyst in PEMFC,' Microporous and Mesoporous Materials, 134(1-
730 3), (2010), 1-7.
731 7. Z. Lei, An. L. Dang, M. Zhao, J. Shi, S. Bai, Y. Cao, 'Highly dispersed platinum supported on nitrogen-
732 containing ordered mesoporous carbon for methanol electrochemical oxidation,' Microporous and
733 Mesoporous Materials, 119(1-3), (2009), 30-38.
734 8. M-K. Min, J. Cho, K. Cho, H. Kim, 'Particle size and alloying effects of Pt-based alloy catalysts for fuel cell
735 applications,' Electrochimica Acta, 45(25-26), (2000), 4211 - 4217.
736 9. G.C. Bond, Heterogeneous Catalysis, 2nd Ed., 1987: Oxford Science Publications.
737 10. L. Guczi, 'Bimetallic nano-particles: featuring structure and reactivity,' Catalysis Today, 101(2), (2005), 53-
738 64.
739 11. J.T. Hwang, J.S. Chung, 'The morphological and surface properties and their relationship with oxygen
740 reduction activity for platinum-iron electrocatalysts,' Electrochim. Acta, 38(18), (1993), 2715-2723.
741 12. P. Gallezot, A. Alarcon-Diaz, J.-A. Dalmon, A.J. Renouprez, B. Imelik, 'Location and dispersion of platinum in
742 PtY zeolites,' Journal of Catalysis, 39, (1975), 334-349.
743 13. D.R. Rolison, E.A. Hayes, W.E. Rudzinski, 'Electrode-modified zeolites: Electrode microstructures contained
744 in and on a heterogeneous catalyst,' Journal of Physical Chemistry, 93(14), (1989), 5524 - 5531.
745 14. T. Yakoyama, N. Kosugi K. Asakura Y. Iwasawa H. Kuroda 'Temperature dependence of the Pt L_3-edge EXAFS
746 of platinum clusters supported on NaY-zeolite,' Journal De Physique, Colloque C8, December 1986, C8-273.
747 15. M.S. Tzou, B.K. Teo, W.M.H. Sachtler, 'Formation of Pt particles in Y-type zeolites: The influence of
748 coexchanged metal cations,' Journal of Catalysis, 113(1), (1988), 220 - 235.

749 16. Z.C. Zhang, T.T. Wong, W.M.H. Sachtler, 'The effect of Ca^{2+} and Mg^{2+} ions on the formation of electron-
750 deficient palladium-proton adducts in zeolite Y,' Journal of Catalysis, 128(1), (1991), 13-22.
751 17. B.I. Boyanov, T.I. Morriso, 'Support and Temperature Effects in Platinum Clusters. 1. Spatial Structure,'
752 Journal of Physical Chemistry, 100(40), (1996), p.16310.
753 18. P. Ueda, T. Kusakari, K. Tomishige, K. Fujimoto, 'Nature of Spilt-over Hydrogen on Acid Sites in Zeolites:
754 Observation of the Behavior of Adsorbed Pyridine on Zeolite Catalysts by Means of FTIR,' Journal of Catalysis,
755 194(1), (2000), 14-22.
756 19. W-J Liu, B-L Wu, C-S Cha, 'Surface diffusion and the spillover of H-adatoms and oxygen-containing surface
757 species on the surface of carbon black and Pt/C porous electrodes,' Journal of Electroanalytical Chemistry,
758 476(2), (1999), 101 - 108.
759 20. L. Persaud, A. J. Bard, A. Campion, M. A. Fox, T. E. Mallouk, S. E. Webber, J. M. White, 'A New Method for
760 Depositing Platinum Exclusively on the Internal Surface of Zeolite L,' Inorg. Chem., 26(22), (1987), 3825-3827.
761 21. P. Gallezot, 'The State and Catalytic Properties of Platinum and Palladium in Faujasite-type Zeolites,'
762 Catalysis Reviews, Science and Engineering, 20, (1979), 121-154. DOI: 10.1080/03602457908065108
763 22. H. Geaischer, C. Tobias, Advances in Electrochemistry and Electrochemical Engineering, Vol. 11, 1978, John
764 Wiley & Sons Inc.
765 23. C.M.A. Brett, A. M. O. Brett, Electroanalysis. 1998: Oxford University Press.
766 24. H.D. Abruna, Electrochemical Interface, Chapter 1: X-Ray Absorption Spectroscopy in the Study of
767 Electrochemical System. 1991, New York: VCH.
768 25. J. Yao, 'Zeolites supported platinum electrocatalysts,' PhD Thesis, Department of Chemistry, University of
769 Southampton (2001).
770 26. R.E. Benfield, 'Mean coordination numbers and the non-metal–metal transition in clusters,' Journal of the
771 Chemical Society, Faraday Transactions, 88, (1992), 1107-1110.
772 27. M.S. Tzou, M. Kusunoki, K. Asakura, H. Kuroda, G. Moretti, W.M.H. Sachtler, 'Bimetallic copper-platinum
773 particles supported in Y zeolite: structural characterization by EXAFS,' J. Phys. Chem., 95(13),)1991), 5210-
774 5215.

775 28. R.J. Mathew, "Towards Time Resolution in EXAFS of Fuel Cell Electrocatalysis", PhD Thesis, Department of
776 Chemistry, University of Southampton (2000).
777 29. M. Fleischmann, S. Pons, D.R. Rolison, P.P. Schmidt (Eds), Ultramicroelectrodes, Data Tech. Science:
778 Morgarcton, NC. 1987.
779 30. L.M. Aparicio, J.A. Dumesic, S.M. Fang, M.A. Long, W.S. Millman, W.K. Hall, 'Mössbauer spectroscopy and
780 catalytic studies of iron-exchanged, silicon-substituted Y-zeolite,' Journal of Catalysis, 104(2), (1987), 381-395.
781 31. S.T. Homeyer, L.L. Sheu, Z.C. Zhang, W.M.H. Sachtler, V.R. Balse, J.A. Dumesic, 'Chemical interaction of
782 palladium particles with iron cations in NaY,' Appl. Catal., 64, (1990), 225-241.
783 32. S. Srinivas, P. Rao, 'Direct Observation of Hydrogen Spillover on Carbon-Supported Platinum and Its
784 Influence on the Hydrogenation of Benzene,' Journal of Catalysis, 148(2), (1994), 470-477.
785 33. J. McBreen, 'Voltammetric Studies of Electrodes in Contact with Ionomeric Membranes,' Journal of The
786 Electrochemical Society, 132(5), (1985), 1112-1116.
787 34. D.W. Breck, Zeolite Molecular Sieves: Structure, Chemistry and Use, Wiley – Inter science Publisher, 1974.
788 35. A. Zhang, I. Nakamura, K. Fujimoto, 'A New Probe Reaction for Studying the Hydrogen Spillover
789 Phenomenon,' Journal of Catalysis, 168(2), (1997), 328-333.